LA-UR-14-27823
Approved for public release; distribution is unlimited.

Title: Molecular dynamics simulations and experimental measurements of UO2 and UO2+x thermal conductivity

Author(s): Andersson, Anders David Ragnar
Liu, Xiang-Yang
Mcclellan, Kenneth James
Lashley, Jason Charles
Byler, Darrin David
Stanek, Christopher Richard
Gofryk, Krzysztof
Tonks, Michael

Intended for: Report

Issued: 2014-11-19 (rev.1)

Molecular dynamics simulations and experimental measurements of UO_2 and UO_{2+x} thermal conductivity

David Andersson, Benjamin Liu, Kenneth McClellan, Jason Lashley, Darrin Byler and Chris Stanek
Los Alamos National Laboratory

Krzysztof Gofryk and Michael Tonks
Idaho National Laboratory

We have performed molecular dynamics (MD) simulations of the UO_2 and UO_{2+x} (x=0.0132, 0.0266, 0.04 and 0.08) thermal conductivities. The results were compared to experimental measurements on single crystal samples with the same oxygen content in order to establish defect scattering parameters due to interstitial oxygen ions and U^{5+} ions on the cation sublattice. The measurements were performed from 4 K to room temperature, which enables us to separate phonon and spin scattering contributions. We also compare to existing experimental data above 500 K [1]. UO_{2+x} is used as surrogate for UO_2 containing irradiation induced defects. The goal is to validate the MD simulations, which can then be used to perform simulations for irradiated UO_2 with higher confidence. It is much more difficult to perform controlled experimental measurements on the latter materials.

Molecular dynamics simulations

In non-metallic solids, phonons dominate thermal transport. This provides the basis of the MD methodology used to predict thermal conductivity. In this study we have employed the non-equilibrium MD method, which is often referred to as the "direct method" [2-4]. In this method, a heat current (J) is applied to the system, and the thermal conductivity k is computed from the time-averaged temperature gradient ($\partial T / \partial z$) from Fourier's law,

$$\kappa = -\frac{J}{\partial T / \partial z} \quad (1)$$

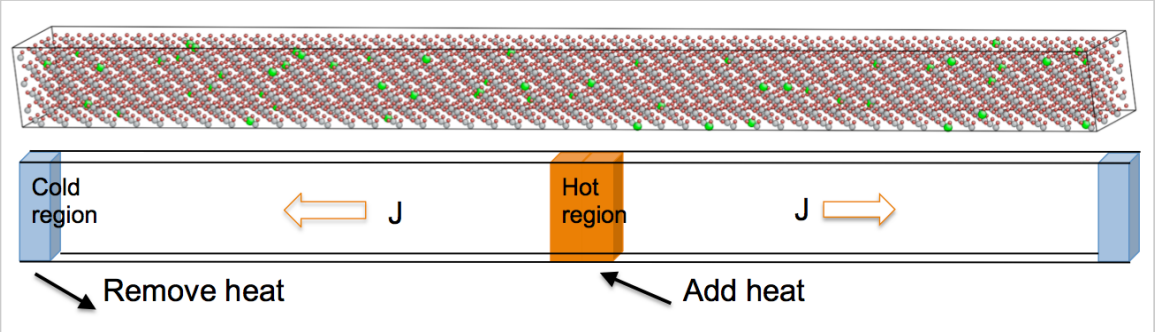

Figure 1. A schematic drawing illustrating the computational setup of non-equilibrium MD simulations of thermal conductivity in UO_{2+x}.

In Figure 1, the computational setup is illustrated, which is identical to that used by us for defect free UO_2 and UO_2 containing fission products. A supercell containing $n_1 \times n_2 \times n_3$ cubic unit cells of UO_2 is constructed. Periodic boundaries are applied in all three dimensions. The heat flow is in the z direction. A cold / hot region is defined at $z = 0$ / $L_z/2$ measuring 1 nm in width from which heat is removed / added during the simulations, where L_z is the periodic length of the supercell in the z direction. For all MD simulations, n_1 and n_2 are set to 3. The dependence of the computed thermal conductivity on cross sectional area has been shown to be weak [5]. The length L_z in the heat flow direction ranges from 19 to 76 nm for different cases. The thermal conductivity calculations were carried out with the direct method as implemented in LAMMPS package [6]. The system is equilibrated initially for 50 ps in the NVT (constant number, constant volume, and constant temperature) ensemble at desired temperature, followed by another 50 ps in the NVE (constant number, constant volume, and constant energy) ensemble. After that, non-equilibrium MD runs were applied to the system, for a period of 5 – 10 ns. After thermal equilibration, the initial 0.5 ns in the thermal simulation was used to accommodate the transient behavior. After that, the temperature profiles were averaged over the rest of the MD time. There are two types of heat control methods in LAMMPS. One is based on the Muller-Plathe algorithm [3]. In this algorithm, the swap between the coldest particle in the cold region and the hottest atom in the hot region is used to remove / add heats to the corresponding regions. By controlling the frequency of swaps during MD, the heat flux between the hot and the cold regions is controlled at the desired level. The other heat control algorithm is based on the method of Jund and Jullien [2]. In this scheme, a fixed amount of energy (ΔE) is added / subtracted from the hot / cold region by velocity rescaling for every MD time step while preserving the total momentum ($\vec{P} = \sum_{i=1,N} m_i \vec{V}_i$) of the atoms in the region, so that

$$\vec{V}_i^{New} = \vec{V}_i + (1-\alpha)\frac{\vec{P}}{\sum m_i} \qquad (2)$$

$$\alpha = \sqrt{1 \pm \frac{\Delta E}{E_k - \frac{1}{2}\sum m_i V_G^2}} \; ; \; V_G = \frac{\left|\vec{P}\right|}{\sum m_i} \qquad (3)$$

The original Jund and Jullien algorithm was derived for a single species system. We found that it applies to multiple species systems as well. Another constant heat flux algorithm using velocity rescaling from Ikeshoji and Hafskjold [4], which was originally derived for multiple species system, is also widely used. These two algorithms are not equivalent, reflecting different flavors in the formulation since the mathematical solution of constant energy change while preserving momentum in a given region is not unique. We found that a precise control of the heat flux is important for studying the length dependence of the thermal conductivity. However, the control of the heat flux by using Muller-Plathe algorithm for given swap frequency is not good since the result depends on other simulation conditions. For

this reason, the method of Jund and Jullien is adopted in all of our MD simulations. The heat flux used in the simulations is 0.001 – 0.002 eV/A per time step, where A is the cross section area of the simulation cell.

The Buckingham type of empirical potential is used to describe the U^{4+} - O^{2-} [7], O^{2-} - O^{2-} [8] interactions in UO_2. For computational efficiency, the Wolf summation [9] is used to compute the long-range Coulombic interactions. For defect calculations, the effect of U^{5+} ions on the cation sublattice due to the O interstitials is not taken into account at the moment. The computational supercells were initially set to the optimized lattice constant 0.5469 nm (0.5456 nm in the Basak potential case). NPT (constant number, constant pressure, and constant temperature) simulations were carried out to determine the thermal expansions at different temperatures. The supercell dimensions were averaged over 100 ps, and the thermal expansion strains are 0.001865 (0.003004), 0.003803 (0.006231), 0.005827 (0.009728), 0.007905 (0.013508), 0.010089 (0.017626) at 300, 600, 900, 1200, and 1500 K for Buckingham (or Basak) potential. All thermal conductivity MD simulations were carried out with the thermal expansion taken into account.

To fit the temperature profiles, a least-squares fit for the linear regression is used. The temperature profiles were fitted in the ranges $w < z < L_z/2 - w$, and $L_z/2 + w < z < L_z - w$, with the choice of the excluded width w as 0.26, in agreement with earlier studies [10]. The obtained gradients from left and right slopes in the temperature profiles are then averaged to determine the thermal conductivity.

MD simulations of pure UO_2 and UO_{2+x} were carried out using both Buckingham potential and Basak potential, at 100, 300, 900 and 1500 K. At each temperature, a set of simulations at different lengths were performed, 19, 24, 32, 49, and 65 nm. The relatively short supercells used in the current MD simulation setups give rise to significant portion of the phonons propagating ballistically through the system, but scatter from the hot and cold plates. This is especially the case for UO_2 where defect scattering is negligible at low temperature, while UO_{2+x} is less sensitive. This causes the thermal conductivity obtained from MD simulations to be lower than they should be. The conventional method to extrapolate the value to an infinitely large system is based on a linear formula,

$$\frac{1}{\kappa} = \frac{1}{\kappa_\infty} + \frac{c}{L_z} \qquad (4)$$

where c is a constant related to scattering by the hot and cold plates, L_z is the length of the simulation cell and κ is the thermal conductivity for a simulation cell of infinite length. As shown in our recent work [17], we found that a quadratic correction is sometimes needed in order to take non-linear effect in the UO_2 lattice into account, which brings the fitting formula to a more general one,

$$\frac{1}{\kappa} = \frac{1}{\kappa_\infty} + \frac{c_1}{L_z} + \frac{c_2}{L_z^2} \qquad (5)$$

where c_1 and c_2 are both constants.

The thermal conductivity κ_∞ for UO_2 and UO_{2+x}, extrapolated from MD results at different sample lengths using the above methodology, is shown in Figure 2, at different temperatures. The present simulations were performed for supercells with the elongated direction coinciding with the [100] direction of the fluorite lattice.

The MD simulations for pure UO_2 overestimate the thermal conductivity compared to experiments, especially at low temperature, see Figure 2. As recently shown, this is due to resonant scattering of phonons by spins in the paramagnetic phase of UO_2 [11], which is not captured by the MD simulations. However, we can correct this deficiency by using the phonon-spin scattering contribution (labeled phonon-magnetic scattering in Figure 2) derived from experimental data [11]. The phonon-spin scattering relaxation time is derived from the experimental data shown in Figure 3a by fitting the data points to the Callaway model [12] including a term for the phonon-spin scattering. This relaxation time is then added to the total relaxation time derived for the MD results using the same Callaway model, but obviously without the phonon-spin contribution. As shown in Figure 2, this approach significantly improves the agreement with experiments for pure UO_2. We can apply the same methodology to correct the MD predictions for UO_{2+x}. The results are shown in Figure 3.

The thermal conductivity of UO_{2+x} has been investigated in several molecular dynamics studies [13-15]. The results show significant variability, which can be ascribed to the empirical potential used to describe the interatomic forces. The study by Watanabe et al. [13] on UO_{2+x} used a renormalization correction to the thermal conductivity results from MD simulations to obtain better agreement with experiments, which was derived by comparing predicted and measured thermal expansion measurements. The physical original of this correction is the spin-phonon interaction applied directly in the present study.

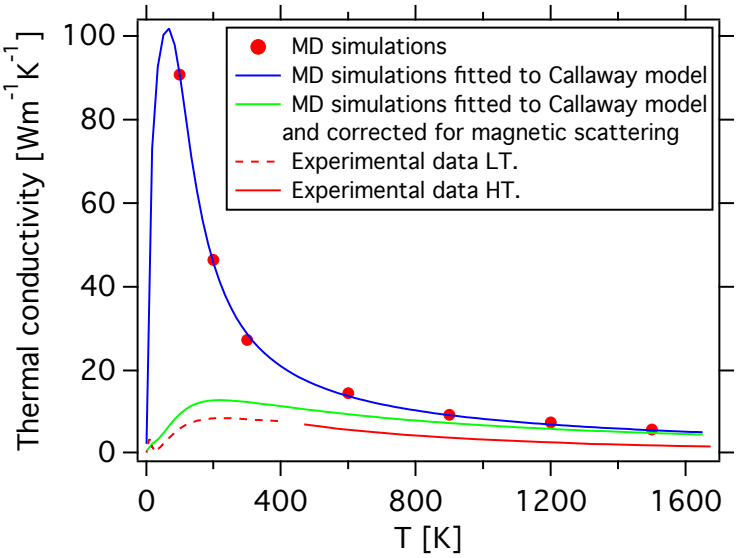

Figure 2. MD simulation of the UO_2 thermal conductivity, both with and without correction for resonant spin-phonon scattering. The spin-phonon scattering correction was derived by fitting a Callaway model to the experimental data [11] and then adding the spin-phonon relaxation time to the MD results. The high temperature experimental data are taken from [1] and the low temperature data from [11].

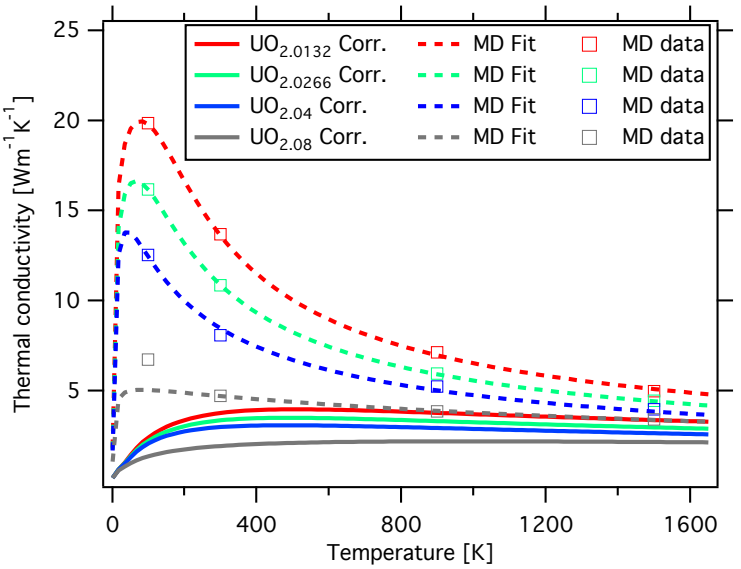

Figure 3. MD simulation of the impact interstitial oxygen (UO_{2+x}) atoms on thermal conductivity, both with (solid lines) and without (dashed lines) correction for resonant spin-phonon scattering. Lines represent Callaway fits to the MD data points (squares). The spin-phonon scattering correction was derived by fitting a Callaway model to the experimental data [11] and then adding the spin-phonon relaxation time to the MD results.

Experimental samples

The depleted UO_2 single crystals used for the thermal conductivity measurements were obtained by Los Alamos Scientific Laboratory (LASL, now Los Alamos National Laboratory, LANL) from Battelle Northwest Laboratory in 1969. Samples were prepared by fusing depleted PWR-grade UO_2 powder in an arc furnace and large crystals were harvested from the bulk [16]. Before delivery to LASL, crystals were annealed in moist hydrogen to remove inclusions and assure stoichiometry. We performed thermal gravimetric analysis (TGA) on the samples studied and the results confirmed original assertion of stoichiometry to be <2.001 (original coulometric titration in 1969 resulted in a stoichiometry of 2.0006). Regarding chemical purity, analysis performed at the time of original synthesis confirmed high purity samples (> 99.9688 %). By emission spectrographic analysis Ag, B, Fe, Sn, etc. were below 200 ppm total, C 50 ppm, Cl less than 10 ppm and F less than 2 ppm. The total nitrogen content was found to be 50 ppm as determined by Kjeldahl analysis. The isotopic purity of the samples was ^{238}U >99.78% (the balance is ^{235}U). Optical microscopy showed the samples to be free of macroscopic defects (cracks, etc.). Oriented rectangular cuboids were prepared from a large single crystal and orientations were verified by standard Laue back-reflection X-ray techniques. The character of the pattern highlights the high quality of the crystal. The UO_{2+x} sample was prepared from the same single crystal by oxidation in controlled gas (H_2, H_2O, O_2, Ar) environment specified by the known UO_{2+x} thermodynamics. The stoichiometry was verified by thermogravimetry measurements. All samples used in the present study were oriented in <111> directions.

Thermal conductivity measurements

The UO_2 and UO_{2+x} thermal conductivity measurements were performed in a Physical Property Measurement System (PPMS-9) from Quantum Design (QD) equipped with a 9 T superconducting magnet and using samples with typical dimensions of ~ 1 × 1 × 7 mm. Both four-terminal and two-terminal probe lead configurations were used to measure thermal conductivity. A silver-filled H20E epoxy was used to connect the sample to the leads, which are gold-coated copper. We used the continuous mode (0.1 $Kmin^{-1}$). In order to gain down the bridge, it is important to use 40 mV as the upper power limit because the resistivity of the sample is in the kOhm regime (at room temperature). According the QD handbook the typical accuracy, taking into account radiation losses, of thermal conductivity measurements using a TTO option is ±5%. However, since our measurements are performed on the same material, having almost the same geometry, the relative accuracy between the samples is much higher. In order to ensure that the sample mounting, e.g. the leads attached to the ends of the UO_2 samples, did not bias the results, we demounted the samples, annealed in H_2 gas to ensure sample stoichiometry, remounted the sample and repeated the thermal conductivity measurements, which reproduced the original results. The variation was well within the uncertainty range of the methodology. The second measurement series used two instead of four wire terminals.

We also compare our MD results to the high temperature measurements by White and Nelson [1]. This study used laser flash analysis method and differential scanning calorimetry to obtain the UO_{2+x} thermal conductivity. The measurements were performed on polycrystalline samples prepared and measured under controlled gas atmosphere to maintain correct stoichiometry. The low temperature thermal conductivity measurements for the [111] orientation on single crystals match the corresponding high temperature polycrystalline measurements by White and Nelson [1] well, see Figure 2.

Comparison between MD predictions and experiments

The MD simulations for UO_{2+x} (corrected for resonant spin-phonon scattering) are compared to experimental measurements in Figure 4. At this point we only have one oxidized sample ($UO_{2.04}$) for the low temperature single crystal measurements but additional results will be available shortly. White and Nelson [1] reported the thermal conductivity for a range a UO_{2+x} stoichiometries at high temperature. Above ~800 K the MD simulations overestimate the thermal conductivity, while it is underestimated below this temperature. The change in thermal conductivity with increasing oxygen content is correctly reproduced in each temperature range. One complication in comparing the MD and experimental results is the strong tendency of UO_{2+x} to phase separate into UO_2+U_4O_9. The transition to a single UO_{2+x} phase occurs at ~800 K and is responsible for the kink in the experimental thermal conductivity measurements. The mixed UO_2+U_4O_9 phase has much higher thermal conductivity than the corresponding disordered UO_{2+x} phase, which is understood in terms of the increased point defect scattering in UO_{2+x} compared to UO_2. U_4O_9 has very low thermal conductivity, as indicated by the experimental data for $UO_{2.21}$. The MD simulations model a perfectly disordered UO_{2+x}, which is only relevant well above 800 K. The UO_2+U_4O_9 phase separation explains why the MD thermal conductivity is lower than the experimental results below 800 K. In agreement with the results for stoichiometric UO_2, the MD simulations seem to slightly overestimate the thermal conductivity above 800 K even after correcting for spin-phonon scattering. We believe that this is a consequence of the empirical potential employed in this study. Other models for the interatomic forces should be employed in future work to assess the sensitivity to the potential employed. In this context, note that the overestimation is very similar in magnitude to the comparison between theory and experiments for stoichiometric UO_2. Consequently, this discrepancy may be inherited from the empirical potential description of UO_2 rather than from the scattering properties of interstitial oxygen ions. The MD simulations reproduce the trend that as the oxygen content increases the thermal conductivity almost reaches a constant value as function of temperature.

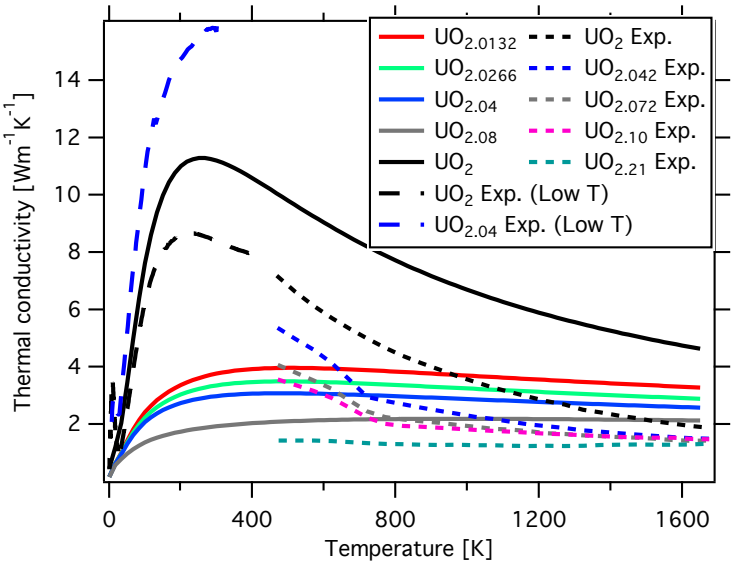

Figure 4. Comparison of the UO_{2+x} thermal conductivity obtained from MD simulations and from experiments. The high temperature experimental data were taken from White and Nelson [1] and the low temperature data are from the present study (UO_{2+x}) or from Gofryk *et al.* [11] (UO_2). The low temperature experimental data were obtained by measurements on single crystals oriented in the [111] crystallographic direction.

The low temperature single crystal measurement on $UO_{2.04}$ gives a very surprising result. The room temperature thermal conductivity is almost twice the value for stoichiometric UO_2, which defies our simple picture of interstitial oxygen ions being scattering centers acting independently of the spin degrees of freedom reducing the thermal conductivity in stoichiometric UO_2. Below the Neel temperature the UO_2 and $UO_{2.04}$ thermal conductivities are much closer, indicating that the increase in thermal conductivity for $UO_{2.04}$ in the paramagnetic phase could be related to changes in the spin scattering mechanism. This interpretation is speculative at this point. If there is a strong coupling between these two scattering mechanisms, the molecular dynamics simulations including the current approach to correct them for missing spin-phonon scattering would not be sufficient. Additional work is required to resolve this issue.

Conclusions

Molecular dynamics (MD) simulations of the UO_2 and UO_{2+x} (x=0.0132, 0.0266, 0.04 and 0.08) thermal conductivities were performed and compared to experimental data collected in the low (<300 K) and high temperature (>500 K) range. The molecular dynamics simulations were corrected for missing spin scattering, as established in previous studies. Above ~800 K the MD simulations overestimate the thermal conductivity, while it is underestimated below this temperature. The change in thermal conductivity with increasing oxygen content is correctly reproduced in each temperature range. At 800 K UO_{2+x} transitions from a two-phase UO_2+U_4O_9 mixture to a UO_{2+x} solid solution, which explains the overestimation/underestimation below/above this temperature as compared to

experiments. Future work will assess the sensitivity of the absolute thermal conductivity values to the potential employed. The low temperature measurements on $UO_{2.04}$, very surprisingly, show increased thermal conductivity above the Néel temperature compared to stoichiometric UO_2. This may indicate a strong coupling between scattering by interstitial oxygen ions and spin-phonon scattering. Additional work is required to resolve this problem.

References

[1] J. T. White and A. T. Nelson, J. Nucl. Mater. **443**, 342 (2013).
[2] P. Jund and R. Jullien, Phys. Rev. B **59**, 13707 (1999).
[3] F. Muller-Plathe, J. Chem. Phys. **106**, 6082 (1997).
[4] T. Ikeshoji and B. Hafskjold, Mol. Phys. **81**, 251 (1994).
[5] X. W. Zhou, S. Aubry, R. E. Jones, A. Greenstein and P. K. Schelling, Phys. Rev. B **79**, 115201 (2009).
[6] http://lammps.sandia.gov.
[7] G. Busker, A. Chroneos, R. W. Grimes and I. W. Chen, J. Am. Ceram. Soc. **82**, 1553 (1999).
[8] R. W. Grimes, J. Am. Ceram. Soc. **77**, 378 (1994).
[9] D. Wolf, P. Keblinski, S. R. Phillpot and J. Eggebrecht, J. Chem. Phys. **110**, 8254 (1999).
[10] P. C. Howell, J. Comput. Theor. Nanos. **8**, 2129 (2011).
[11] K. Gofryk, S. Du, C. R. Stanek, J. C. Lashley, X. -Y. Liu, R. K. Schulze, J. L. Smith, D. J. Safarik, D. D. Byler, K. J. McClellan, B. P. Uberuaga, B. L. Scott and D. A. Andersson, Nature Commun. **5**, 4551 (2014).
[12] X. Y. Liu, D. A. Andersson, B. P. Uberuaga, J. Mater. Sci. **47**, 7367 (2012).
[13] T. Watanabe, S. G. Srivilliputhur, P. K. Schelling, J. J. S. Tulenko, S. B. Sinnott and S. R. Phillpot, J. Am. Ceram. Soc. **92**, 850 (2009).
[14] S. Nichenko and D. Staicu, J. Nucl. Mater. **433**, 297 (2013).
[15] S. Yamasaki, T. Arima, K. Idemitsu, and Y. Inagaki, Int. J. Thermophys. **28**, 661 (2007).
[16] W. Ellis and R. Schwoebel, Surf. Sci. **11**, 82 (1968).